# NMR-directed design of pre-TCRβ and pMHC molecules implies a distinct geometry for pre-TCR relative to αβTCR recognition of pMHC

Robert J. Mallis[‡], Haribabu Arthanari[‡§], Matthew J. Lang[¶], Ellis L. Reinherz[‖], and Gerhard Wagner[‡1]

From the [‡]Department of Biological Chemistry and Molecular Pharmacology, Harvard Medical School, Boston, Massachusetts 02115, [§]Department of Cancer Biology, Dana–Farber Cancer Institute, Boston, Massachusetts 02115, [¶]Department of Chemical and Biomolecular Engineering, Vanderbilt University and Department of Molecular Physiology and Biophysics, Vanderbilt University School of Medicine, Nashville, Tennessee 37235, and [‖]Department of Medical Oncology, Laboratory of Immunobiology, Dana–Farber Cancer Institute and Department of Medicine, Harvard Medical School, Boston, Massachusetts 02115

Edited by Wolfgang Peti

The pre-T cell receptor (pre-TCR) guides early thymocytes through maturation processes within the thymus via interaction with self-ligands displayed on thymic epithelial cells. The pre-TCR is a disulfide-linked heterodimer composed of an invariant pre-TCR α (pTα) subunit and a variable β subunit, the latter of which is incorporated into the mature TCR in subsequent developmental progression. This interaction of pre-TCR with peptide-major histocompatibility complex (pMHC) molecules has recently been shown to drive robust pre-TCR signaling and thymocyte maturation. Although the native sequences of β are properly folded and suitable for NMR studies in isolation, a tendency to self-associate rendered binding studies with physiological ligands difficult to interpret. Consequently, to structurally define this critical interaction, we have re-engineered the extracellular regions of β, designated as β-c1, for prokaryotic production to be used in NMR spectroscopy. Given the large size of the full extracellular domain of class I MHC molecules such as H-Kᵇ, we produced a truncated form termed Kᵇ-t harboring properties favorable for NMR measurements. This system has enabled robust measurement of a pre-TCR–pMHC interaction directly analogous to that of TCRαβ–pMHC. Binding surface analysis identified a contact surface comparable in size to that of the TCRαβ–pMHC but potentially with a rather distinct binding orientation. A tilting of the pre-TCRβ when bound to the pMHC ligand recognition surface *versus* the upright orientation of TCRαβ would alter the direction of force application between pre-TCR and TCR mechanosensors, impacting signal initiation.

αβT cell–mediated immunity serves to combat cellular-based pathologies that afflict the vertebrate host, including those caused by viruses and cancers. At the core of T cell recognition and activation function is the surface T cell receptor (αβTCR),[2] consisting of a clone-specific TCRαβ heterodimer and invariant dimeric CD3 signaling subunits (CD3εγ, CD3εδ, and CD3ζζ) that are non-covalently associated to form an eight-transmembrane-component complex. TCRαβ recognizes "foreign" peptides derived from proteins unique to a pathogenic process such as a viral protein or mutated host gene product within a transformed cell. A key feature of this recognition is that a peptide is presented in the context of peptide-major histocompatibility complex (pMHC) molecules on the surface of the abnormal cell or cross-presented on dedicated antigen-presenting cells that acquire the protein and surface-array the peptide. The pathogenically derived foreign pMHCs must be recognized in the context of tens of thousands of self-pMHCs generated as a result of the breakdown of endogenous proteins that are displayed on the same host cell. This discrimination is tuned through the harnessing of external cellular forces generated as a T cell scans its environment for foreign pMHC during immune surveillance as well as through the actuation of intracellular cytoskeletal forces that dynamically tune immune recognition (1–5). Indeed, it appears that the T cell utilizes piconewton-level forces to initiate signaling-linked structural transitions that extend TCR–pMHC bond lifetime (1, 4, 6, 7), although the atomistic details of this are yet to be fully resolved.

The requirement for exquisite ligand discrimination, to selectively sense foreign pMHC over self-pMHC, drives selection processes in thymocyte development to eliminate αβTCRs with excess self-reactivity without removing those harboring the potential to bind foreign peptides. This is no simple task as a protective αβTCR should recognize self-MHC molecules while distinguishing foreign peptides from self-peptides in the groove of the self-MHC molecule. This is more difficult consid-

ering that at the TCR–pMHC interaction surface the TCR makes many more atomic contacts with the MHC than with the peptide.

The pre-TCR pTα-β heterodimer is an obligate precursor to TCRαβ in the development of αβ T cells (8). Pre-TCRs express the somatically rearranged TCRβ gene product, the β subunit, paired with an invariant pTα subunit, itself comprising a single Cα-like constant domain and lacking a variable domain and associated complementarity-determining regions (CDRs), which drive ligand recognition within TCRαβ. Nevertheless, the pre-TCR is itself a fully functional receptor that includes the same CD3 subunits to initiate signaling (6, 9). Both the CDR loops of Vβ and a hydrophobic patch on Vβ, exposed as a consequence of being in an unpaired V module topology, mediate ligand binding to pMHC (9). The self-pMHC interaction specificity of the pre-TCR drives expansion of the CD4⁻CD8⁻ double-negative thymocytes (6, 9) and appears to foster preferential expansion of those thymocytes that recognize peptides in the context of self-MHC. Furthermore, the relaxed peptide specificity of the pre-TCR relative to the αβTCR that appears at the CD4⁺CD8⁺ double-positive thymocyte stage has also been observed and is consistent with the notion of pre-TCR introducing a self-MHC bias (6, 10, 11). Following pre-TCR-driven β chain selection, the αβTCR replaces the pre-TCR, and each TCR clonotype rigorously selects for a precise peptide specificity using its paired VαVβ module. Desirable TCRs undergo positive selection (survival), whereas harmful (strongly autoreactive) TCRs undergo negative selection (deletion) at the CD4⁺CD8⁺ double-positive stage and/or further developmental stages (8, 12–14).

Because the pre-TCR plays a major role in this two-step T cell repertoire refinement, we sought to characterize the binding event between β and pMHC to decipher the parameters of this recognition relative to those of the TCRαβ–pMHC interaction (9). More importantly, we would like to delineate differences between the pre-TCR and the αβTCR recognition events to better understand the biological function of the pre-TCR while providing new insights into TCR function (3, 4, 6). Due to inherent self-association of component molecules (15) and the large size of the complex, attempts to fully define the interactions have been difficult (9, 15). We therefore designed a model system to explore the pre-TCR–pMHC interaction in atomic detail. Experiments presented here establish a working model of the pre-TCR–pMHC interaction through the design of a modified β chain (9) and a truncated mutant of pMHC (16) to describe the pre-TCR–pMHC interaction surfaces.

## Results

### Interaction of pMHC with the β subunit of the pre-TCR is hampered by self-association of β through the constant domain

In an attempt to characterize an interaction between a β chain and a pMHC, we utilized two distinct β chains with only 34% sequence identity within their Vβ regions, N30β and N15β, for which the αβTCR of each recognizes the same pMHC, a vesicular stomatitis virus nucleoprotein octapeptide bound to H-2K$^b$ (VSV8/K$^b$) (9, 17, 18). Each β subunit pro-

motes β selection in thymic culture systems (9) and could potentially provide complementary information on the pre-TCR–pMHC complex. We first added unlabeled VSV8/K$^b$ to a purified ¹⁵N-labeled sample of N30β and acquired ¹H-¹⁵N HSQC spectra with transverse relaxation optimized spectroscopy (TROSY) selection of the mixture and compared it with a spectrum of N30β. Utilizing the backbone assignments of N30β (18), we were able to determine the interaction site by mapping the combined ¹H-¹⁵N chemical shift changes (CCSCs) on a previously determined X-ray crystallographic model (15) (Fig. 1, *A* and *B*). The largest chemical shift changes were not localized to any single site on the surface of N30β but did cluster in the C domain at the conserved Cα- or pTα-Cβ interface (19, 20). Additional changes were seen in the C domain AB and EF helices, which are located proximal to the C terminus of the TCR. There were some scattered changes within the V domain, but these were not clustered as tightly as those identified in the C domain. This result suggested that any V domain interaction was weaker than the nonspecific interactions within the C domain, which is not known to interact with pMHC in the TCRαβ, making it unlikely that we were observing physiologically relevant interactions. To understand whether the C domain–mediated nonspecific interactions were a general phenomenon, we next studied the interaction of pMHC with N15β. Because N15β is known to self-associate (15) via Vβ, we used cross-saturation transfer (CST) NMR experiments, which highlight only regions of heteromolecular association, in contrast to chemical shift perturbation analyses, which also highlight changes in surfaces due to self-association or allosteric changes. In CST experiments, the observed protein is ¹⁵N-labeled and perdeuterated, which implies that it will have no resonances in the aliphatic region of the ¹H NMR spectrum. The binding partner, in this case pMHC, will be protonated and will harbor resonances in the aliphatic region, but because this protein is not ¹⁵N-labeled it will be invisible in a ¹⁵N HSQC spectrum. In CST experiments, we selectively magnetize the unlabeled protein and monitor transfer of magnetization to the labeled protein, which will reveal the direct interaction interface. In the case of N15β, we found a significant CST effect in the Vβ as well as Cβ (Fig. 1, *C* and *D*). Because the pre-TCR contains a pTα subunit that lacks a Vα-like subunit (Fig. 2*A*), we posit that the changes seen in the V domain were more physiologically relevant than those seen in the C domain (20).

### Structure-aided design of β as a pre-TCR model

Fig. 2*A* shows the overall topology of the pre-TCR pTα-β heterodimer (20), illustrating that the interaction surfaces highlighted in the N15β-VSV8/K$^b$ interaction are occluded by pTα in the C domain but are not occluded in the V domain (Fig. 1, *C* and *D*). When examining the crystallographic model of the pre-TCR, we noted a hydrophobic cluster, including residues Phe-131, Val-147, and Leu-149 that are occluded in the pre-TCR (Fig. 2*B*). We hypothesized that mutating the equivalent residues in N15β or N30β would abrogate the interaction within this non-physiologically relevant binding surface. It was thus clear that to accurately judge the binding capacity of TCRβ, measuring only interaction potential of elements exposed on cell surfaces, we needed to remove the non-physiologic inter-
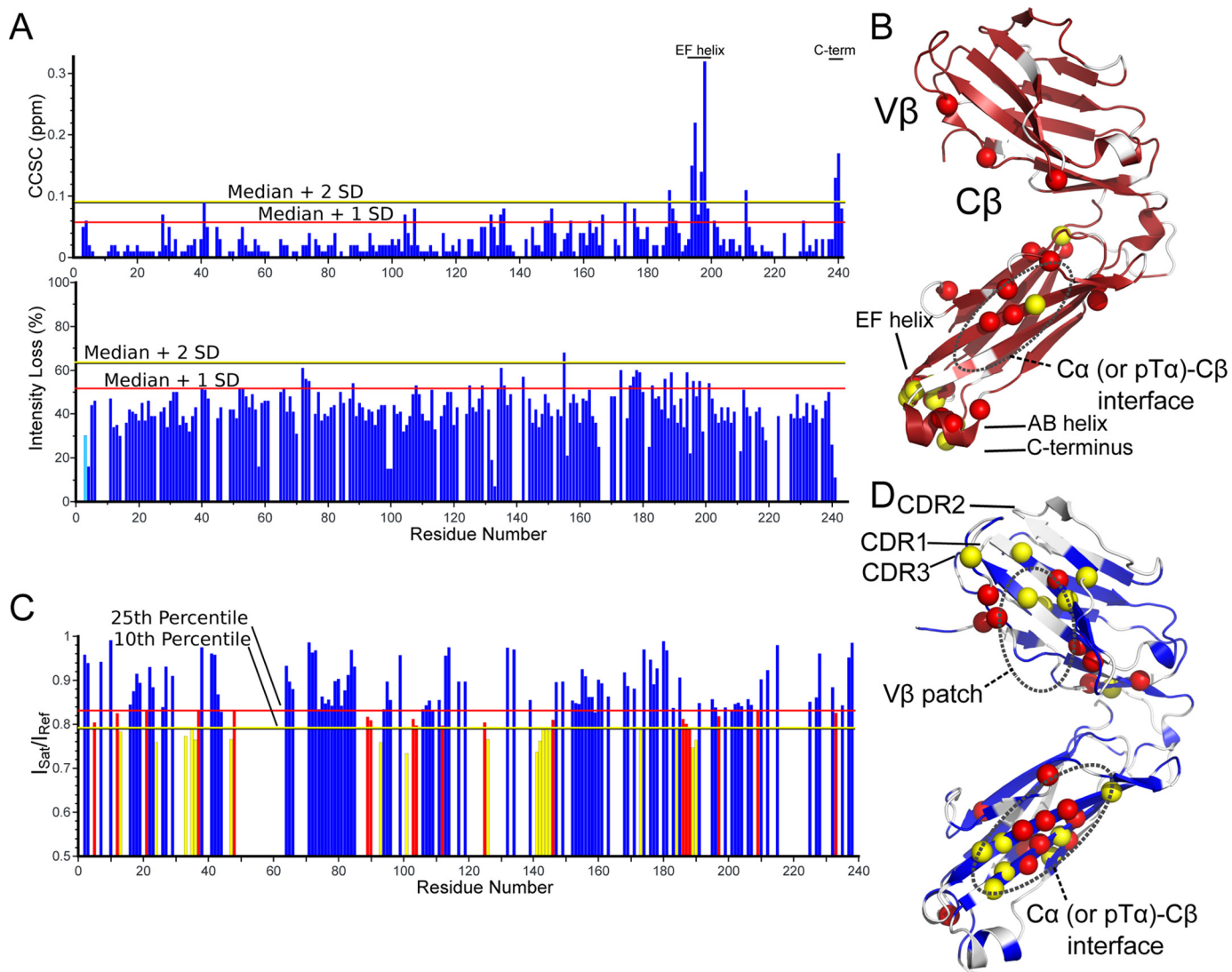
⧟ASBMB

*J. Biol. Chem.* (2018) 293(3) 754–766 **755**

**Figure 1. Interaction of TCRβ with pMHC via C domain.** *A–D*, N30β (*A* and *B*) or N15β (*C* and *D*) interacts with VSV8/Kᵇ via elements of Cβ. Schematic diagrams show residues that are impacted by addition of VSV8/Kᵇ as *spheres*. *A*, plot of combined ¹H-¹⁵N CCSC (*top* plot) or intensity loss (*bottom* plot) *versus* residue number upon addition of 500 μM VSV8/Kᵇ to 200 μM ¹⁵N-labeled N30β. Cutoff values of median + 1 or 2 S.D. are indicated as are regions of largest perturbations. Residue A3 increased in intensity by 30% and is shown in *cyan*. *B*, residues that exhibit chemical shift perturbation (median + 1 S.D., *red spheres*; median + 2 S.D., *yellow spheres*) are indicated on the structure of N30β (Protein Data Bank code 3Q5T). *C*, plot of cross-saturation effect (Iₛₐₜ/Iᵣₑf) *versus* residue with addition of 350 μM VSV8/Kᵇ to 175 μM ²H/¹³C/¹⁵N-labeled N15β. Residues that exhibit significant cross-saturation effect (top 10th (*yellow bars*) or 25th percentile (*red bars*)) are highlighted. *D*, residues that exhibit significant cross-saturation effect (top 10th (*yellow spheres*) or 25th percentile (*red spheres*)) with addition of 350 μM VSV8/Kᵇ to 175 μM ²H/¹³C/¹⁵N-labeled N15β are indicated on the structure of N15β (Protein Data Bank code 3Q5Y).

action within the Cβ interface normally contacting Cα or pTα (19, 20). Due to the placement of the hydrophobic residues Phe-131, Val-147, and Leu-149 in β-sheet secondary structures, we chose replacements with known β-strand–forming propensities (21), F131R, V147Q, and L149Q, each of which places a charged or hydrophilic residue at this interface.

### Mutagenesis of Cβ

The ¹⁵N HSQC spectrum of the N30β mutant F129R/V145Q/L147Q, denoted N30β-c1, is quite similar to that of the WT (Fig. 2*C*) as is the case with N15β F128R/V144Q/L146Q (N15β-c1) compared with WT (Fig. 2*D*), indicating an overall similar fold of the molecule. When examining residues in the Cβ domain of N30β-c1, these resonances are shifted compared with those in N30β, whereas those in the V domain remain unchanged (Fig. 2*E*), indicating that any changes due to the

mutation are local and do not affect V domain–binding regions. We conclude that the replacement of the Phe/Val/Leu hydrophobic cluster resulted in a β chain with a fold similar to that of the WT (9, 18).

### Rotational correlation time (τ_c) measurements show diminished self-association in β-c1

Using NMR, one can measure relaxation rates from which molecular correlation times such as $\tau_c$ can be extracted. The $\tau_c$ may report on the oligomeric states of the observed protein, in solution, at the given concentration and in equilibrium where the interacting partners are not distinguished. Utilizing transverse relaxation correlation time (TRACT) experiments (22), we were able to measure $\tau_c$ values, which are positively correlated to the apparent size of a molecule, inclusive of oligomeric state, for N30β and N15β (Fig. 2*F*). $\tau_c$ increased with increasing
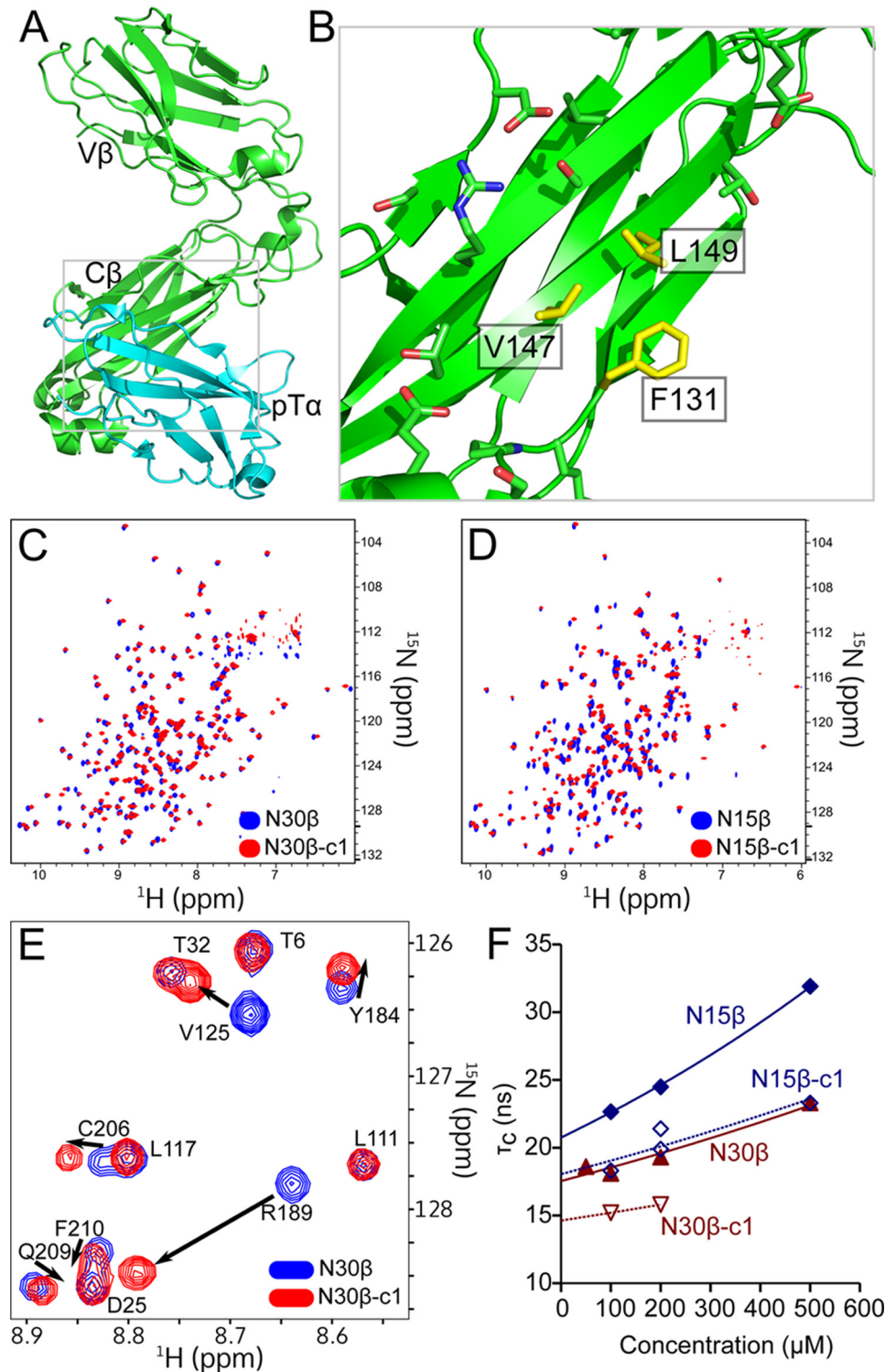
**Figure 2. Mutagenesis targets within the pre-TCR β subunit.** *A*, pre-TCR crystal structure model (Protein Data Bank code 3OF6) in schematic representation in the same orientation as Fig. 1*B*. *B*, expanded view of *boxed* area of *A* showing only TCRβ. The view is rotated ~15° about *x* and *y* to highlight the contact surface. Side chains of residues contacting (*i.e.* within 4 Å of) pTα are shown in *stick* representation. Three hydrophobic residues targeted for mutagenesis are colored *yellow*. Numbering is according to that found in the crystal structure 3OF6 and is offset from those of N15 and N30β by three or two residues, respectively. *C* and *D*, overlay of $^1$H-$^{15}$N TROSY-HSQC of N30β (18) and N30β-c1 (9) (*C*) or N15β (18) and N15β-c1 (9) (*D*) to illustrate similarity of spectra. *E*, region of overlaid spectra shown in *C* with labeled peaks indicating lack of chemical shift changes in the V domain (Thr-6, Thr-32, Asp-25, Leu-111, and Leu-117), whereas those in the C domain (Val-125, Tyr-184, Arg-189, Gln-209, and Phe-210) show significant changes. *F*, rotational correlation times of WT and mutant TCRβs suggest abrogation of self-association within Cβ. The plot shows $\tau_c$ *versus* concentration for N15 (*blue diamonds*) and N30β (*red triangles*). *Lines* show exponential fits of points to guide the eye. WT is shown with *filled symbols* and *solid lines*, and c1 mutants are shown with *open symbols* and *dotted lines*.
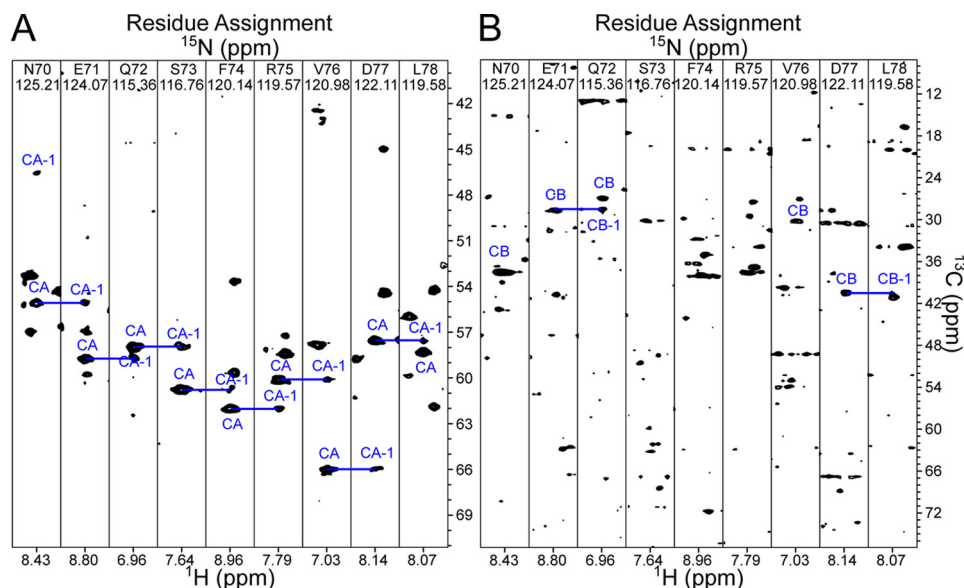
**Figure 3. Three-dimensional correlations for backbone assignment of VSV8/K$^b$.** *A*, selected regions of the HNCA experiment illustrating the quality of the spectrum for a given section within the $\alpha$1 helix. *B*, selected regions of the HNCACB experiment for the same region as in *A*.

concentration for each protein, ranging from 18 to 23 ns for N30$\beta$ at 50–500 $\mu$M, whereas N15$\beta$ varied from 23 to 32 ns over similar concentrations. At the lowest concentrations measured here, the $\tau_c$ was 18.6 and 22.7 ns. These values were greater than the predicted value of 16.3 ns for these 27-kDa proteins as calculated using the software HYDRONMR (23). Although we cannot rule out self-association via V$\beta$, we posit that at least part of this self-association is the result of intermolecular interactions of C$\beta$ (15). N15$\beta$ self-associates more than N30$\beta$ ($p = 0.028$), supporting the idea that N15$\beta$ utilizes the V domain more in self-association. $\tau_c$ for N30$\beta$-c1 was found to be 15.2 and 15.8 ns for 100 and 200 $\mu$M samples, respectively (Fig. 2*F*). This is consistent with essentially monomeric TCR$\beta$ as determined from hydrodynamic radius calculations using HYDRONMR (23) wherein a value of 16.3 ns is predicted for the 27-kDa monomer. This supports the idea that N30$\beta$-c1 exists as a monomer at these concentrations and self-associates significantly less than WT ($p = 0.035$). In contrast, N15$\beta$-c1 exhibits an increase in $\tau_c$ at concentrations from 100 to 500 $\mu$M (Fig. 2*F*) with values comparable with those seen for the WT N30$\beta$ but significantly less self-association than WT N15$\beta$ ($p = 0.032$). It is expected that N15$\beta$-c1 continues to self-associate more than N30$\beta$-c1 ($p = 0.042$) because X-ray crystallographic analyses have revealed V$\beta$-V$\beta$ association in N15$\beta$-c1, whereas N30$\beta$-c1 contained contacts mainly utilizing C$\beta$ (15). This analysis also agrees with observations that N15$\beta$ will utilize the V$\beta$ hydrophobic patch more readily in the context of pre-TCR recognition of pMHC (9).

### Backbone resonance assignments of full-length VSV8/K$^b$

In our previous study, we were able to demonstrate an interaction between N15$\beta$-c1 and labeled K$^b$ within the VSV8/K$^b$ complex (9). To characterize the binding site on pMHC, we required the backbone resonance assignment of VSV8/K$^b$. Utilizing non-uniform sampling (24), we collected high resolution TROSY versions of HNCA/HNCOCA/HNCO/HNCACO/

HNCACB spectra on perdeuterated $^2$H/$^{13}$C/$^{15}$N-labeled heavy chain with perdeuterated but otherwise unlabeled $\beta_2$-microglobulin ($\beta_2$m), the smaller protein subunit of the MHC heterotrimer, and unlabeled VSV8. As shown in Fig. 3*A*, signals of cross-peaks were quite strong in the HNCA experiment with signals for both the HN correlated and its preceding (*i* and *i* − 1, respectively) residue in each spin system. Conversely, for the HNCACB (Fig. 3*B*), most spin systems lack cross-peaks for Cb$_{i − 1}$, whereas ~30% lack cross-peaks for Cb$_i$. Similarly, the HNCO experiment provided robust Co$_{i − 1}$ cross-peaks, whereas the HNCACO lacked cross-peaks for most Co$_i$ resonances. Because of the sparse coverage in sequential connectivities, we pursued orthogonal means of backbone assignment using the program RASP (25) to iteratively utilize chemical shift predictions to find potential resonance assignments. These assignments were cross-checked manually against a high-resolution $^{15}$N dispersed TROSY-HSQC-NOESY experiment for confirmatory cross-peaks indicative of through-space contacts. This procedure was critical in assigning the $\beta$-sheet that forms the base of the peptide-binding groove and those that comprise the $\alpha$3 domain and allowed the completion of 73% of the non-proline backbone amide resonance assignments (Fig. 4*A*). Depicted in Fig. 4, *B* and *C*, is the completeness of assignment overlaid on the X-ray structure of VSV8/K$^b$ (26). Notably, the $\alpha$2 helix, proximal to the peptide-binding loop, with a likely role in pre-TCR binding, remained largely unassigned. Whether this is related to the specific peptide in the MHC groove or a more common feature of K$^b$ *per se* requires further study but implies that mobility in this region might have important consequences for dynamics of $\alpha\beta$TCR–pMHC as well as pre-TCR–pMHC interaction.

### Large size of VSV8/K$^b$–N15$\beta$-c1 complex impacts measurement of binding interface

The backbone assignments were then used to interpret the previously reported $^1$H-$^{15}$N TROSY-HSQC measurement of
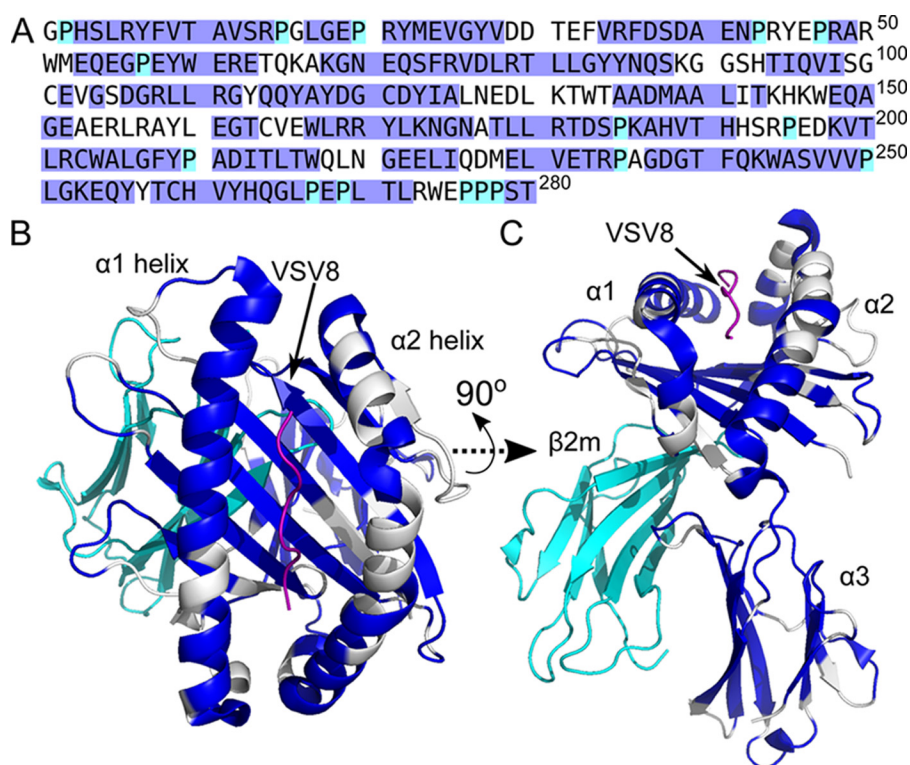
**Figure 4. Backbone assignment of VSV8/Kᵇ.** *A*, amino acid sequence of Kᵇ. Highlighted in *blue* are assigned residues. *Cyan* indicates the positions of unassigned Pro residues. Completeness of assignment is of 194 of 264 non-proline residues (73%). *B* and *C*, VSV8/Kᵇ structural model (Protein Data Bank code 1KPU) with assigned residues within Kᵇ colored *blue*, unassigned residues and prolines colored *white*, VSV8 in *purple*, and β₂m in *cyan*. *C* is rotated by 90° about the *x* axis relative to *B*.

unlabeled N15β addition to VSV8/Kᵇ wherein the heavy chain of Kᵇ was ¹⁵N-labeled (9). As shown in Fig. 5A, chemical shift perturbation data analysis suggests a binding interaction involving the canonical peptide-binding groove previously reported for all TCRαβ–pMHC interactions. However, the data are not unequivocal, with a number of residues distal to the canonical surface and within the α3 subunit revealing changes similar to those seen at the putative interfacial region. The regions associated with the largest peak intensity losses (Fig. 5B) conform to the region surrounding the peptide, clustering more closely to the canonical binding interface. Whether due to the large size of the complex or the weak nature of the binding event, a more precise interaction map could not be obtained. This, combined with the incomplete assignment of the region surrounding the peptide-binding pocket, led us to attempt to engineer improvements in the biophysical behavior of the pMHC complex.

### Engineering a truncated pMHC model

The inability to obtain the complete backbone resonance assignments of the receptor-binding portion of the MHC may have been due to the large size of the pMHC complex or the conformational heterogeneity within the complex. TRACT measurements of VSV8/Kᵇ at 100 $\mu$M indicate a $\tau_c$ of 32 ns, corresponding to a predicted molecular mass of 85 kDa for a spherical molecule, nearly double that of the 45-kDa monomeric pMHC. This long correlation time may be caused by the oblong shape of the molecule but regardless explains quite well the poor quality of the triple-resonance backbone experiments. To

obtain more complete backbone assignments while improving the quality of spectra when measuring the β-pMHC complex, we designed a truncated Kᵇ molecule (termed Kᵇ-t) lacking the α3 domain and β₂m (16). TRACT measurements at 67 $\mu$M indicate that VSV8/Kᵇ-t is monomeric with a $\tau_c$ of 15 ns, corresponding to an expected molecular mass of 28 kDa, which is in better agreement with its molecular mass of 22 kDa.

### Backbone resonance assignment of VSV8/Kᵇ-t

We proceeded to assign backbone resonances for ²H/¹³C/¹⁵N-labeled VSV8/Kᵇ-t, acquiring triple-resonance experiments as for the full-length VSV8/Kᵇ. The HNCA shows a complete cross-peak complement for each HN-correlated spin system (Fig. 6A) as does the HNCACB (Fig. 6B). This allowed a more facile assignment of the majority of HN resonances present within the TROSY-HSQC spectrum, assigning 139 of 178 non-proline residues (78%; Fig. 7A). Surprisingly, similar to the full-length VSV8/Kᵇ (Fig. 4), the α2 helix flanking the peptide-binding groove remained recalcitrant to assignment with 19 residues within the α2 helix as well as nine more directly contacting this region remaining unassigned. We suspect, given the high quality of the spectra as well as the known mobility of the α2 helix (27), that this inability to assign this region of the protein reflects an intermediate (~ms–s)-timescale motion (28) on the part of the peptide and α2 helix, broadening these resonances. That it is unassigned in both full-length and truncated constructs argues that this is an intrinsic property of the molecule and not the result of experimental manipulation.
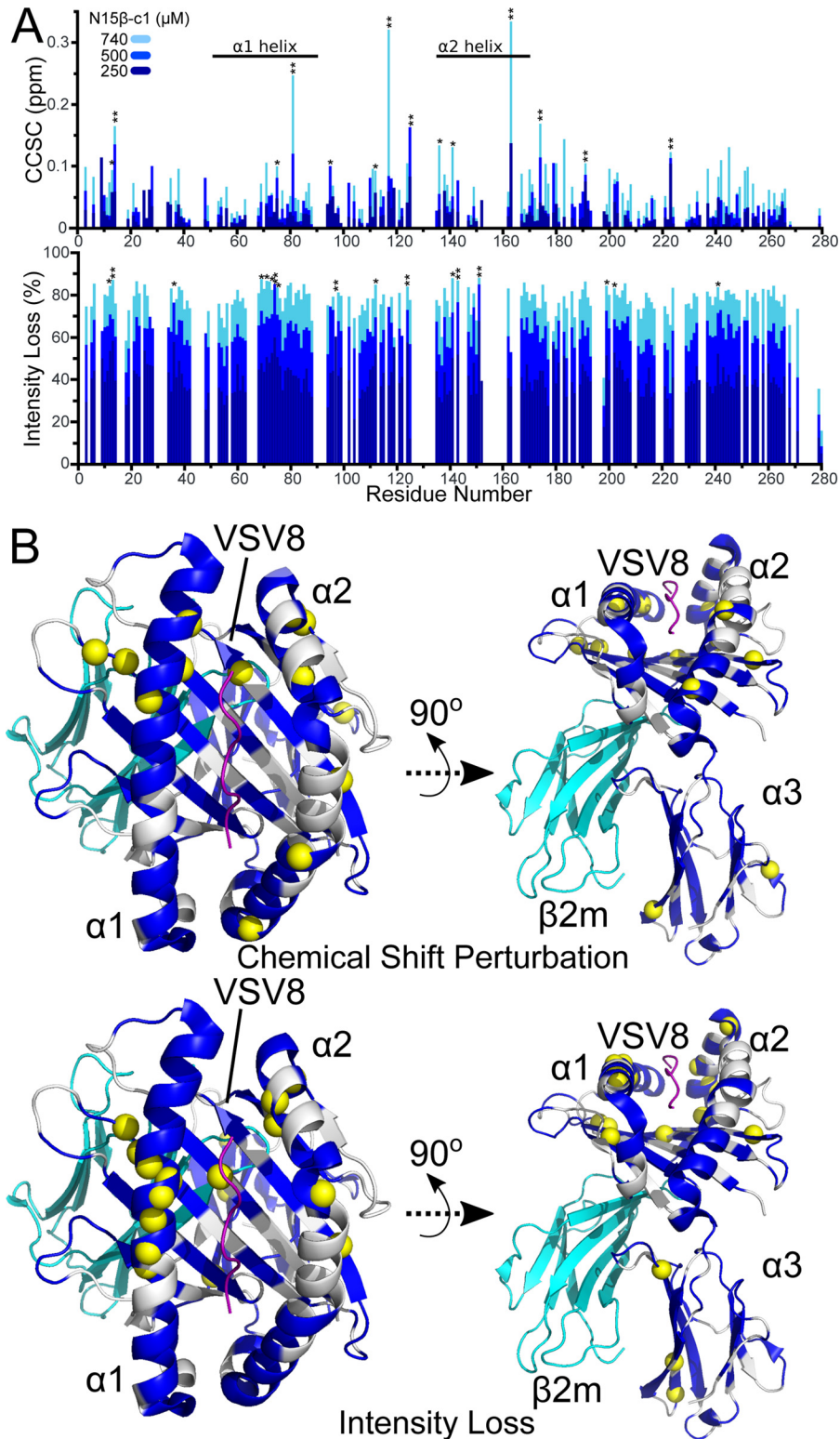
**Figure 5. Interaction of VSV8/Kᵇ with N15β-c1.** *A*, CCSC (*top*) or intensity loss (*bottom*) of ¹⁵N-labeled Kᵇ within VSV8/Kᵇ complex using data published in Mallis *et al.* (9) wherein 200 (*dark blue*), 500 (*blue*), or 750 (*cyan*) μM N15β-c1 was added to 200 μM VSV8/Kᵇ. Residues that differ at the $p < 0.01$ (**) or $p < 0.05$ (*) level between the measured value for that residue and the median value for each experiment are indicated. *B*, residues with significant changes from median values of chemical shift changes (*top row*) or intensity losses (*bottom row*) depicted in *A* are shown as *yellow spheres* on the structural model of VSV8/Kᵇ.

## N15β-c1 recognizes VSV8/Kᵇ-t via CDR and Vβ patch region

As the truncated Kᵇ construct appeared folded in a manner consistent with the fold of the full-length heterotrimeric mole-

cule, we tested pre-TCR recognition of VSV8/Kᵇ-t by incubation with ¹⁵N-labeled N15β-c1. Spectral changes (Fig. 8A) are consistent with the binding event reported previously (9) with
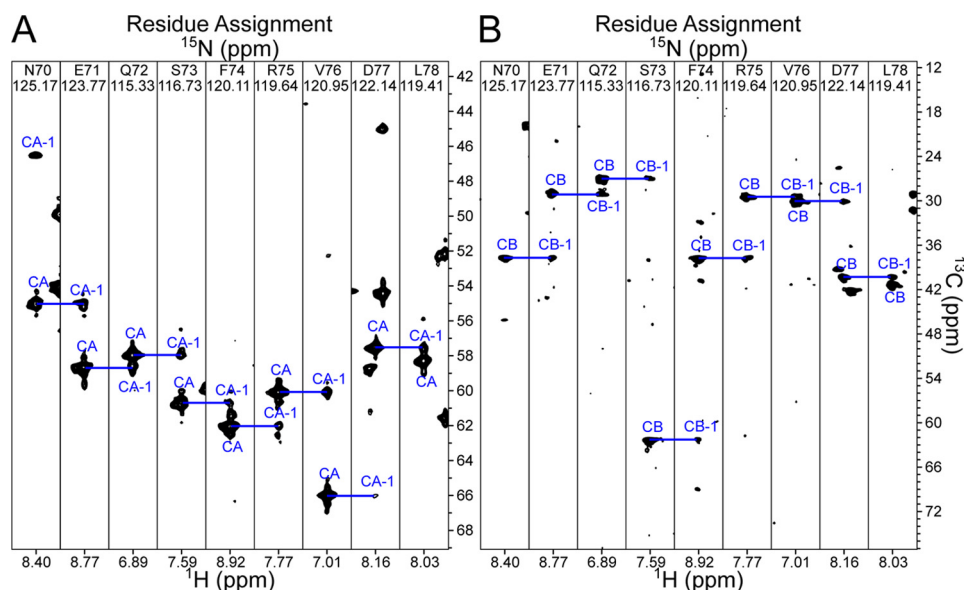
**Figure 6. Three-dimensional correlations for backbone assignment of VSV8/K$^b$-t.** *A*, selected regions of the HNCA experiment illustrating the quality of the spectrum for a given section within the α1 helix. *B*, selected regions of the HNCACB experiment for the same region as in *A*. The same residues were used here as in Fig. 3.
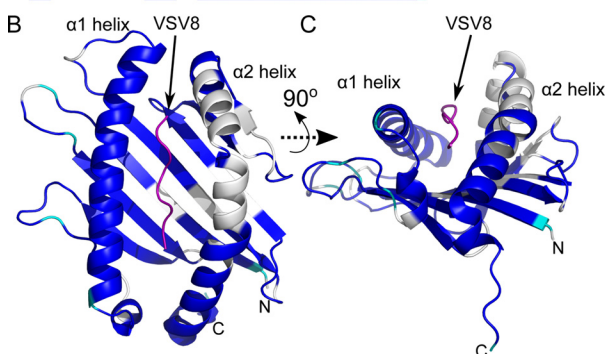


**Figure 7. Backbone assignment of VSV8/K$^b$-t.** *A*, amino acid sequence of K$^b$-t. Highlighted in *blue* are assigned residues. *Cyan* indicates the positions of unassigned Pro residues. Completeness of assignment is 78% non-proline residues. *B* and *C*, VSV8/K$^b$ structural model (Protein Data Bank code 1KPU) with assigned residues within K$^b$ colored *blue*, unassigned residues in *white*, prolines in *cyan*, and VSV8 in *purple*. *C* is rotated by 90° about the *x* axis relative to *B*.

chemical shift and intensity changes consistent with binding kinetics in the fast-to-intermediate exchange regime (28). The changes are almost exclusively located in Vβ (Fig. 8, *B* and C) with significant overlap between regions with chemical shift perturbation and intensity loss. The largest chemical shift and intensity changes are located in the CDR1 and -3 loops as well as Vβ patch region. Note that the CDR2 loop is not assigned likely due to conformational exchange. A region with smaller chemical shift changes is found distal to the interaction surface but still within Vβ, clustered within a region encompassing residues 15–25 (the AB loop and B strand) and residues 74–85 (E strand and EF loop). These changes may occur as a result of secondary rearrangements within the binding interface and are consistent with a dynamic view of pre-TCR or TCR interactions with pMHC (4, 6, 9, 18, 29). The magnitude of chemical shift

changes are similar when 200 μM N15β-c1 is added to full-length VSV8/K$^b$ compared with VSV8/K$^b$-t with the 95th percentile of CCSC equal to 0.064 (9) *versus* 0.060, respectively. Peak intensity losses, as expected, were lower overall due to the smaller size of the β-pMHC complex when truncated pMHC was used with median intensity loss (thus measuring residues not directly interacting with TCRβ) of 27 *versus* 47% (9) when the full-length MHC is utilized. Less overall peak broadening allowed more precision in measuring peak positions for chemical shift perturbation analysis and allowed a greater dynamic range for distinguishing exchange broadening leading to peak intensity losses (Fig. 8, *B* and *C*).

### Pre-TCR recognizes a surface similar to TCRαβ on pMHC

Because we were able to assign a significant portion of the putative interface, we proceeded to measure $^1$H-$^{15}$N TROSY-HSQC spectra of $^1$H/$^{15}$N-labeled K$^b$-t bound to unlabeled VSV8. With titration of unlabeled N15β-c1, we measured chemical shift changes and intensity losses within K$^b$-t (Fig. 9, *A and B*). We observed significant chemical shift changes localized to the α1 helix, which comprises residues 57–85, and assigned portions of the α2 helix, which comprises residues 138–176, as well as residues forming the "floor" of the peptide-binding groove (Fig. 9, *C and D*). Despite the lack of assignments within the α2 helix and the peptide VSV8 itself, these chemical shift perturbations define a contiguous binding interface. The chemical shift perturbation map compares favorably with that measured using the full-length K$^b$ molecule (Fig. 5), demonstrating the validity of improvements made by shortening the construct. Indeed, if one overlays the chemical shift perturbation map obtained with the truncated pMHC onto the structure of VSV8/K$^b$ bound to N15αβ (30), the extent of the pre-TCR–pMHC interaction matches with the TCRαβ–pMHC interface determined by X-ray crystallography (Fig. 10). This strongly suggests that the pre-TCR recognizes a similar surface on pMHC as does TCRαβ. To highlight the distinctness
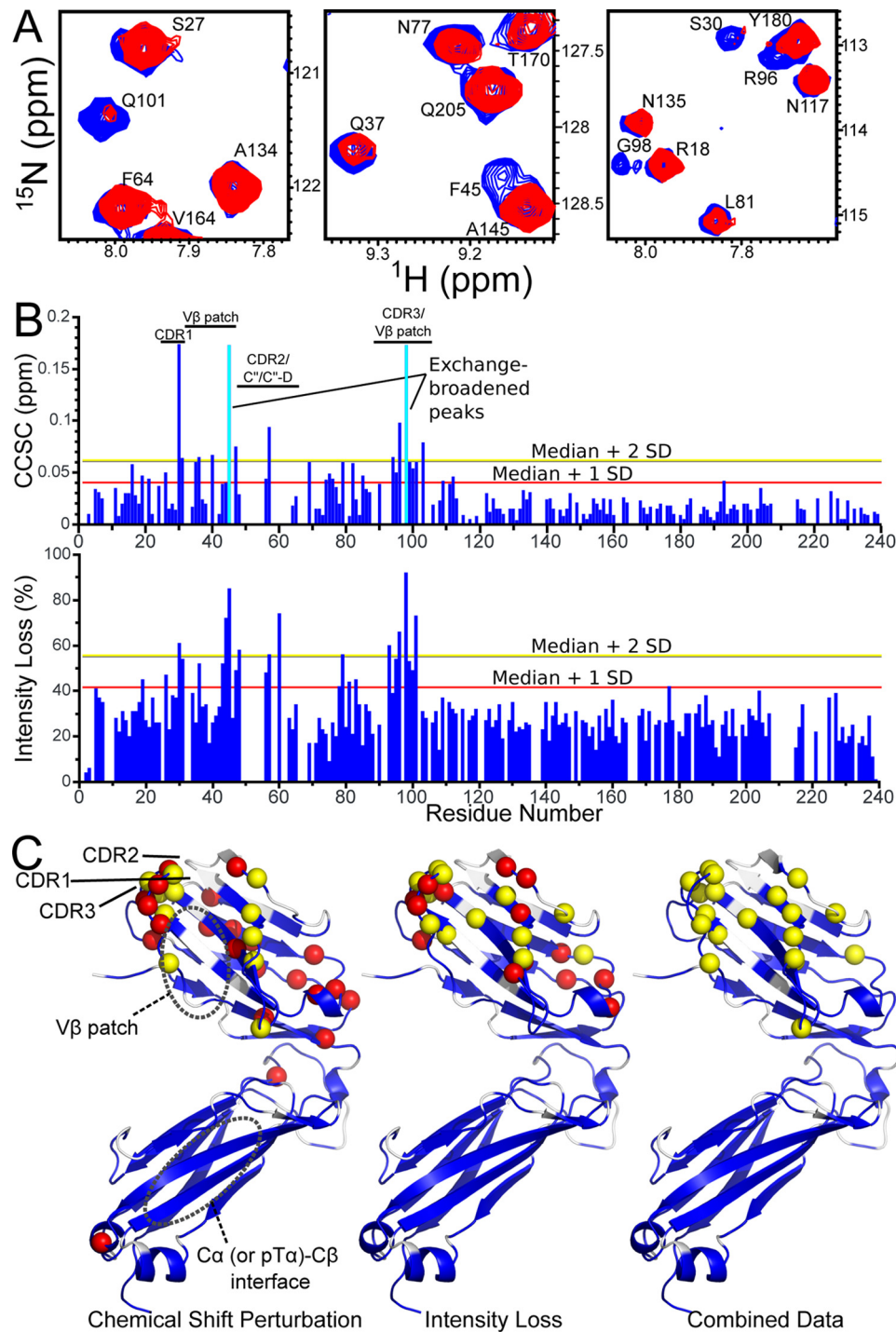
**Figure 8. N15β-c1 binding to VSV8/Kᵇ-t.** *A*, selected regions of ¹H-¹⁵N TROSY-HSQC spectra highlighting changes with addition of unlabeled VSV8/Kᵇ-t to ¹⁵N-labeled N15β-c1. Spectral regions measuring 200 $\mu$M ¹⁵N-labeled N15β-c1 (*blue*) are overlaid with those measuring 200 $\mu$M ¹⁵N-labeled N15β-c1 + 200 $\mu$M VSV8/Kᵇ-t (*red*). CDR residues Ser-30, Arg-96, Gly-98, and Gln-101 as well as Vβ patch residues Gln-37 and Phe-45 are shown exhibiting chemical shift changes, intensity changes, or both. *B*, CCSC (*upper panel*) or intensity losses (*lower panel*) *versus* residue number for spectra outlined in *A*. Residues in which exchange broadening made accurate determination of peak position impossible are indicated by a *cyan bar* in the *upper panel*. *Lines* indicating statistical cutoffs used in structural mapping are shown. *C*, schematic representation of N15β-c1 showing chemical shift perturbation (*left*), intensity loss (*center*), or combined data showing residues two S.D. from median in either measure (*right*). Assigned residues are colored *blue*, and unassigned residues are *white*. Significantly perturbed residues differing from the median by twice the S.D. are highlighted as *yellow spheres*, and those that differ by one S.D. are shown as *red spheres*.

of geometries that the respective interfaces place upon the molecular complex, we utilized HADDOCK2.2 web server (31) to generate a preliminary model of the pre-TCR–pMHC interaction interface (Fig. 10*D*). Given the lack of orientational restraints, it is not surprising that the low-energy conforma-

tions clustered into two distinct docking orientations offset by ~180° as typified by the three lowest-energy conformations shown here. Each of the models utilizes the CDR2 and -3 loops as well as the surface that normally interacts with V$\alpha$ within the $\alpha\beta$ heterodimer, *i.e.* the V$\beta$ patch and surrounding regions. It is
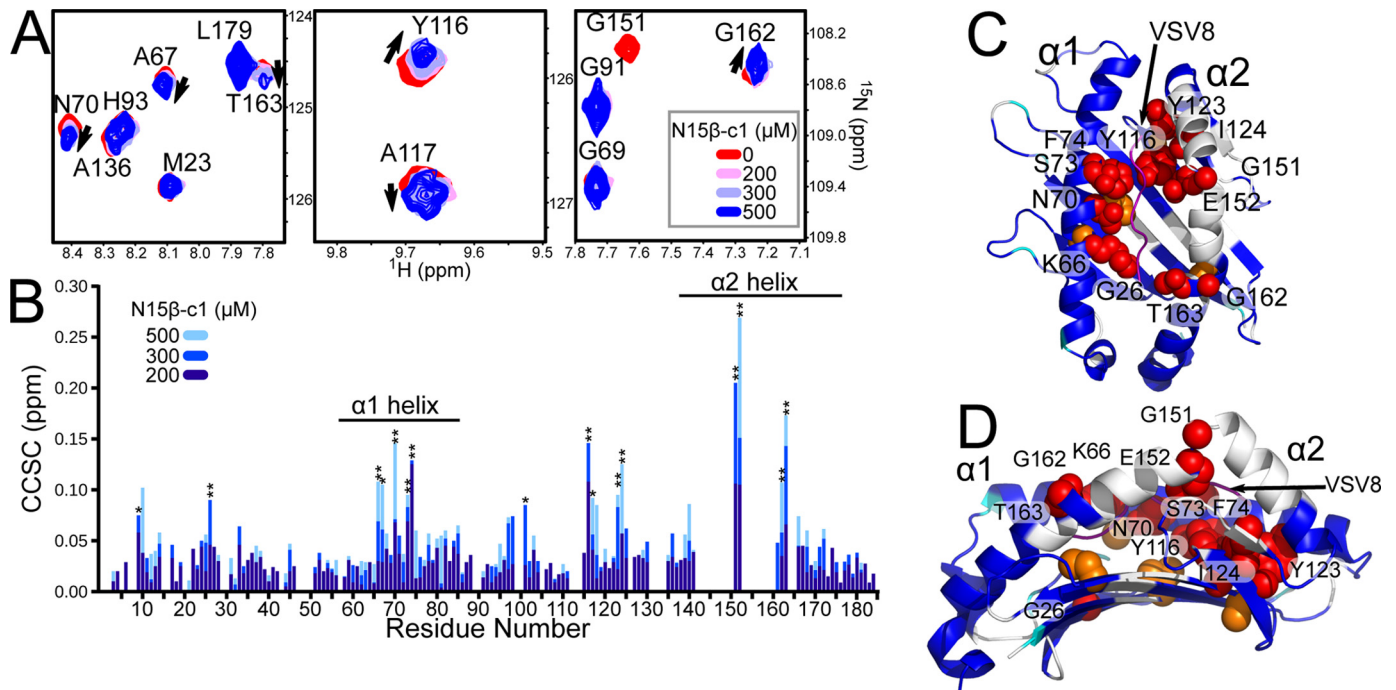
**Figure 9. NMR detection of interaction between N15β-c1 and VSV8/Kᵇ-t.** *A,* selected regions of ¹H-¹⁵N TROSY-HSQC spectra highlighting changes with addition of unlabeled N15β-c1 to ¹⁵N-labeled VSV8/Kᵇ-t. Spectra are overlaid for VSV8/Kᵇ-t alone (*red*) and with addition of 200 (*pink*), 300 (*lavender*), or 500 (*blue*) μM N15β-c1. *B,* CCSCs for spectra outlined in *A* for 200 (*dark blue*), 300 (*blue*), or 500 (*cyan*) μM N15β-c1. Residues that differ at the $p < 0.01$ (**) or $p < 0.05$ (*) level between the CCSC for that residue and the median CCSC for each experiment are indicated. *C* and *D,* schematic representation of VSV8/Kᵇ-t with assigned residues colored *blue,* unassigned residues in *white,* prolines in *cyan,* and VSV8 in *purple.* Significantly perturbed residues by CCSC at $p < 0.01$ are highlighted as *red spheres,* and those that differ at $p < 0.05$ are shown as *orange spheres.* Residue identities are indicated. *D,* view rotated by 90° about the *x* and *y* axes relative to *C* with the α2 helix proximal.
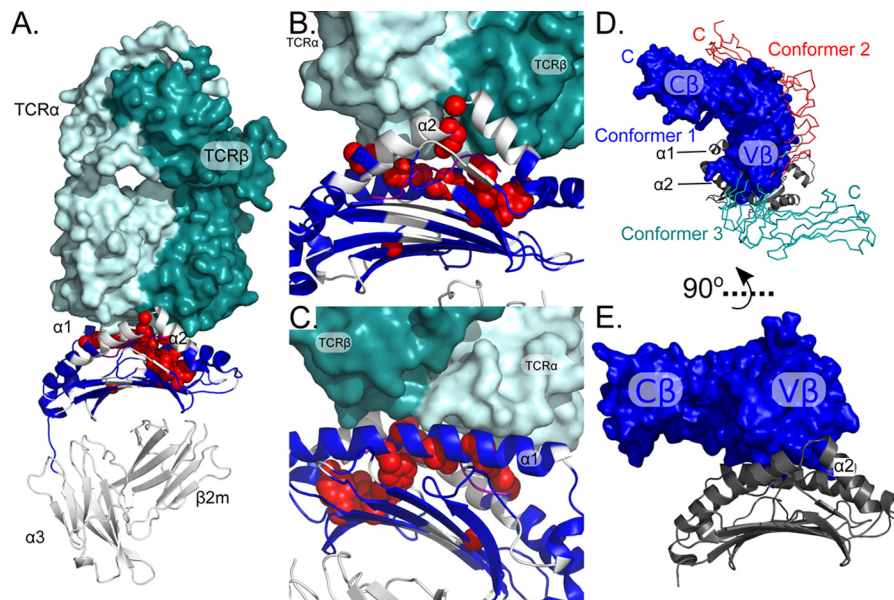


**Figure 10. Modeling pre-TCR–pMHC complex.** *A–C,* location of residues participating in interaction with N15β in the N15β-VSV8/Kᵇ X-ray structure (30). *A,* interacting residues indicated by *red spheres* were defined by CCSC differing at the $p < 0.01$ level between the CCSC for that residue and the median CCSC for each experiment. The VSV8/Kᵇ-t structure is depicted with assigned residues colored *blue,* unassigned residues as well as α3 and β₂m subunits not present in this construct colored *white,* and VSV8 in *purple.* *B* and *C* are zoomed in to highlight the interaction site with α2 proximal in *B* and rotated 180° about the *y* axis and α1 proximal in *C*. *D,* three representative conformers of N15β-c1 interacting with VSV8/Kᵇ as determined by molecular modeling using CST data for the N15β-c1 interaction surface (9) and VSV8/Kᵇ-t CCSC data (Fig. 9) as ambiguous restraints input for HADDOCK2.2 (31). The conformers are representative of the three lowest-energy clusters of binding conformations and are color-coded with one shown as van der Waals surface representation and two shown in ribbon. The Cβ domain membrane-proximal end for each conformer is indicated with a color-coded "C." The models are aligned by overlay of the pMHC, shown in *gray* schematic with α1 and α2 labeled. *E,* side view with only conformer 1 of β shown and differing by a rotation of 90° about the *x* axis relative to *D*. VSV8/Kᵇ-t is in the same approximate orientation as VSV8/Kᵇ shown in *A* with α2 facing front.

likely that interaction of CDR3 and the Vβ patch also requires neighboring CDR2 to participate in the modeled complex despite the absence of NMR-generated constraints. The models

also provide conformations that do not result in obvious clashes with known pre-TCR (15, 20, 32) or pMHC glycosylation sites (33) (Fig. S1). The apposition of these elements results in a more

![ASBMB]

*J. Biol. Chem.* (2018) 293(3) 754–766  **763**

horizontal orientation of the β subunit relative to the MHC peptide-binding groove, suggesting an acute angle of contact between pre-TCR and pMHC. This is readily observed by comparing the long axis of the β subunit shown in Fig. 10*A* with that in Fig. 10*E*.

## Discussion

This study highlights the rational design of recombinant prokaryotically expressed proteins, which in the wild-type form are not ideal for NMR studies. Specifically, domains that self-associate or interact within non-physiologically relevant regions (Figs. 1 and 2) in comparison with their eukaryotically expressed transmembrane protein counterparts were rendered less reactive, whereas proteins that are simply too large for NMR to measure with sufficient precision (Figs. 3–5) have been pared down to their essential components. Structure-based design considerations allowed these hurdles to be overcome, thereby acquiring more accurate measurement of their binding capacity, thus leading to biologically important observations (Fig. 10 and Refs. 6 and 9). TRACT measurements clearly report the predicted decrease in $\tau_c$ and thus apparent molecular size at any given concentration with mutation of Cβ residues. Additionally, the increase of $\tau_c$ with increasing concentration is lesser for the c1 mutant, making readily apparent the difference in molecular behavior conferred by these mutations. Similarly, building on prior design of pMHC for molecular studies (16), we were able to improve an existing model system for NMR study through modification of pMHC (Figs. 6–9).

The chemical shift perturbation analysis of N15β binding to VSV8/K$^b$-t implies a binding mode in which the pre-TCR utilizes a similar binding interface on pMHC as seen for TCRαβ. As shown by the overlay of chemical shift perturbation data for the pre-TCR model with crystallographic data for the TCR system (Fig. 10, *A–C*), the interaction surface is similar between the systems. Once high-resolution structures are available, it will be valuable to compare the determinants of binding for the pre-TCR system *versus* the TCR, particularly focusing on the complementarity of the interacting surfaces as the weaker binding as measured by biomembrane force probe (9) or optical tweezers (6) for the N15β-c1 for VSV8/K$^b$ as compared with that of N15αβ (9) implies suboptimal contacts in the former despite apparently similar contact area with pMHC ligands. The fact that the only other pre-TCR tested, N30β, exhibits even more attenuated binding than N15β (9) suggests that weaker interactions are the norm for pre-TCR. In contrast, we have noted that the pre-TCR–N15β exhibits a force-bond lifetime profile similar to that of the OT1 αβTCR-Ova/K$^b$ system (9). It should be noted, additionally, that there are likely an array of self-pMHCs that are the physiologic ligands for any given pre-TCR (6, 9) and that some may possess as high or even higher affinity than that found for the cognate ligand of the respective TCRαβ. Because of the convoluted and transient procession from thymic progenitor to T cell (34), it may be difficult to define the "true" ligand for any pre-TCR. Although there is good evidence for self-pMHC promotion of pre-TCR–mediated proliferation and progression (6, 9), the existence of non-MHC ligands for pre-TCR (35, 36) has not yet been ruled out.

Meanwhile, as implied by single-molecule studies, the Vβ patch region actively participates in binding by replacing Vα (6). In support of this hypothesis, the molecular modeling using ambiguous NMR restraints (Fig. 10*D*) shows conformations that uniformly predict a more horizontal apposition of pre-TCR to pMHC. In the pre-TCR, the long axis of the β subunit is roughly parallel to the MHC groove, whereas in the TCR it is perpendicular. If this is the case, then this implies an initial contact orientation prior to the application of mechanical force that is rather tilted relative to the more upright TCR when bound to pMHC. This tilted interface would affect the load-sustaining ability and transmission of force through the pre-TCR with implications for the mechanisms of catch-bond formation and mechanical triggering. The sensitivity of pre-TCR–bearing thymocytes to triggering may be potentiated by such a mechanism. It has been seen that the pTα-β is more compliant than the TCRαβ, undergoing a catch-bond requisite reversible transition more readily (6). The unpaired Vβ domain structure in the case of the pre-TCR relative to the paired VαVβ module in the TCRαβ can explain this compliance difference. As we have previously suggested (15), the location of glycans on murine pTα rules out some homodimerization models (20) of pre-TCR function. Although glycan sites do not appear to directly conflict with ligand binding measured here, the proximity of the β chain (Figs. 10, *D* and *E*, and S1) or the pTα subunit (Fig. S1) in these models to the conserved glycan sites on pMHC means that some guiding role for glycan modulation of early thymocyte progression directly through the impact of these interactions or indirectly via recruitment of other cell surface proteins (37) cannot be excluded. The initial pre-TCR structural binding model presented here in conjunction with single-molecule biophysical analysis performed previously (6) suggests that the biology of the pre-TCR and αβTCR will manifest important distinctions built around a common β chain module.

## Experimental procedures

### Protein production

Unlabeled and isotopically labeled N15β, N15β-c1, N30β, and N30β-c1 were produced as detailed (18). Briefly, β chains were expressed using *Escherichia coli* as inclusion body (ib) preparations. These ib preparations were washed thoroughly in 50 mM Tris-Cl, pH 8, 150 mM NaCl (TBS); dissolved in 6 M guanidine hydrochloride; refolded by dilution in 5.4 M guanidine hydrochloride, pH 8, 1 M Arg, 1 mM reduced glutathione, 0.1 mM oxidized glutathione; and subsequent dialysis in TBS. VSV8/K$^b$ was prepared as detailed (9, 38). VSV8 was chemically synthesized (United Biosystems, Inc.), and K$^b$ and β$_2$m were produced via *E. coli* as ib preparations. The ib preparations were washed in TBS and dissolved in 8 M urea. VSV8, Kb, and β$_2$m were mixed in 20 mM Tris-Cl, pH 8, 8 M urea buffer and dialyzed serially against 2, 1, 0.5, and 0 M urea in 20 mM Tris-Cl, pH 8, for 2 h or overnight with a final dialysis against 0 M urea, 20 mM Tris-Cl, pH 8, overnight. VSV8/K$^b$-t was prepared identically to VSV8/K$^b$ with the exception that 1 mM reduced glutathione and 0.1 mM oxidized glutathione were included prior

to dialysis-mediated refolding. Proteins were purified by successive rounds of size-exclusion chromatography.

## NMR

Standard pulse sequences were utilized on Bruker 750-MHz and Varian 600-MHz spectrometers equipped with cryogenically cooled probes or a Bruker 500-MHz spectrometer with a room temperature probe. Concentrations of proteins were in the range of 50–500 $\mu$M, and NMR experiments were conducted at 298 K in PBS (50 mM NaPO$_4$, 150 mM NaCl, pH 7.0) unless otherwise indicated. CCSC was calculated using the formula CCSC = $|5 \times \Delta\delta(^1\text{H})| + |\Delta\delta(^{15}\text{N})|$. All spectra were processed with NMRPipe (39) and visualized using CARA (40).

## Cross-saturation transfer experiments

Unlabeled 175 $\mu$M VSV8/K$^b$ was added to uniformly $^2$H/$^{13}$C/$^{15}$N-labeled 350 $\mu$M N15$\beta$ in PBS (20 mM NaPO$_4$, 50 mM NaCl, pH 7.0) in 80% (v/v) $^2$H$_2$O/H$_2$O. The protonated VSV8/K$^b$ was saturated by an adiabatic WURST (wideband, uniform rate, and smooth truncation) pulse (25 ms) with an excitation bandwidth of 750 Hz. CST experiments were performed in an interleaved fashion with the on-resonance saturation pulse centered at 1 ppm (sat) and the off-resonance saturation pulse centered at −19 ppm (ref). The CST effect was calculated as a ratio of resonance peak intensities (sat/ref). Optimal saturation was found to occur at 3-s saturation time. The top 10th or 25th percentile was taken as the affected region.

## Backbone assignment

TROSY versions of HNCA, HNCOCA, HNCO, HNCACO, and HNCACB (41) were used for backbone assignment of K$^b$ and K$^b$-t. Assignments were completed using CARA (40) in conjunction with RASP (25), utilizing chemical shift predictions generated by SPARTA+ (42).

## Statistical analysis

Statistical significance (*p*) was calculated by linear regression analysis using the R software package (43).

*Author contributions*—R. J. M. conducted experiments, analyzed results, and drafted the paper. R. J. M., H. A., E. L. R., M. J. L., and G. W. conceived the research, planned experiments, analyzed results, and wrote the paper.

## References

1. Kim, S. T., Takeuchi, K., Sun, Z.-Y., Touma, M., Castro, C. E., Fahmy, A., Lang, M. J., Wagner, G., and Reinherz, E. L. (2009) The $\alpha\beta$ T cell receptor is an anisotropic mechanosensor. *J. Biol. Chem.* **284,** 31028–31037 CrossRef Medline
2. Liu, B., Chen, W., Evavold, B. D., and Zhu, C. (2014) Accumulation of dynamic catch bonds between TCR and agonist peptide-MHC triggers T cell signaling. *Cell* **157,** 357–368 CrossRef Medline
3. Brazin, K. N., Mallis, R. J., Das, D. K., Feng, Y., Hwang, W., Wang, J.-H., Wagner, G., Lang, M. J., and Reinherz, E. L. (2015) Structural features of the $\alpha\beta$TCR mechanotransduction apparatus that promote pMHC discrimination. *Front. Immunol.* **6,** 441 CrossRef Medline
4. Das, D. K., Feng, Y., Mallis, R. J., Li, X., Keskin, D. B., Hussey, R. E., Brady, S. K., Wang, J.-H., Wagner, G., Reinherz, E. L., and Lang, M. J. (2015) Force-dependent transition in the T-cell receptor $\beta$-subunit allosterically regulates peptide discrimination and pMHC bond lifetime. *Proc. Natl. Acad. Sci. U.S.A.* **112,** 1517–1522 CrossRef Medline
5. Liu, Y., Blanchfield, L., Ma, V. P., Andargachew, R., Galior, K., Liu, Z., Evavold, B., and Salaita, K. (2016) DNA-based nanoparticle tension sensors reveal that T-cell receptors transmit defined pN forces to their antigens for enhanced fidelity. *Proc. Natl. Acad. Sci. U.S.A.* **113,** 5610–5615 CrossRef Medline
6. Das, D. K., Mallis, R. J., Duke-Cohan, J. S., Hussey, R. E., Tetteh, P. W., Hilton, M., Wagner, G., Lang, M. J., and Reinherz, E. L. (2016) Pre-T cell receptors (pre-TCRs) leverage V$\beta$ complementarity determining regions (CDRs) and hydrophobic patch in mechanosensing thymic self-ligands. *J. Biol. Chem.* **291,** 25292–25305 CrossRef Medline
7. Feng, Y., Brazin, K. N., Kobayashi, E., Mallis, R. J., Reinherz, E. L., and Lang, M. J. (2017) Mechanosensing drives acuity of $\alpha\beta$ T-cell recognition. *Proc. Natl. Acad. Sci. U.S.A.* **114,** E8204-E8213 CrossRef Medline
8. von Boehmer, H., Aifantis, I., Gounari, F., Azogui, O., Haughn, L., Apostolou, I., Jaeckel, E., Grassi, F., and Klein, L. (2003) Thymic selection revisited: how essential is it? *Immunol. Rev.* **191,** 62–78 CrossRef Medline
9. Mallis, R. J., Bai, K., Arthanari, H., Hussey, R. E., Handley, M., Li, Z., Chingozha, L., Duke-Cohan, J. S., Lu, H., Wang, J.-H., Zhu, C., Wagner, G., and Reinherz, E. L. (2015) Pre-TCR ligand binding impacts thymocyte development before $\alpha\beta$TCR expression. *Proc. Natl. Acad. Sci. U.S.A.* **112,** 8373–8378 CrossRef Medline
10. Garcia, K. C., Gapin, L., Adams, J. J., Birnbaum, M. E., Scott-Browne, J. P., Kappler, J. W., and Marrack, P. (2012) A closer look at TCR germline recognition. *Immunity* **36,** 887–888, author reply 889–890 CrossRef Medline
11. Baker, B. M., and Evavold, B. D. (2017) MHC bias by T cell receptors: genetic evidence for MHC and TCR coevolution. *Trends Immunol.* **38,** 2–4 CrossRef Medline
12. Sasada, T., Ghendler, Y., Wang, J. H., and Reinherz, E. L. (2000) Thymic selection is influenced by subtle structural variation involving the p4 residue of an MHC class I-bound peptide. *Eur. J. Immunol.* **30,** 1281–1289 CrossRef Medline
13. Nitta, T., Nitta, S., Lei, Y., Lipp, M., and Takahama, Y. (2009) CCR7-mediated migration of developing thymocytes to the medulla is essential for negative selection to tissue-restricted antigens. *Proc. Natl. Acad. Sci. U.S.A.* **106,** 17129–17133 CrossRef Medline
14. Stritesky, G. L., Xing, Y., Erickson, J. R., Kalekar, L. A., Wang, X., Mueller, D. L., Jameson, S. C., and Hogquist, K. A. (2013) Murine thymic selection quantified using a unique method to capture deleted T cells. *Proc. Natl. Acad. Sci. U.S.A.* **110,** 4679–4684 CrossRef Medline
15. Zhou, B., Chen, Q., Mallis, R. J., Zhang, H., Liu, J.-H., Reinherz, E. L., and Wang, J.-H. (2011) A conserved hydrophobic patch on V$\beta$ domains revealed by TCR$\beta$ chain crystal structures: implications for pre-TCR dimerization. *Front. Immunol.* **2,** 5 CrossRef Medline
16. Jones, L. L., Brophy, S. E., Bankovich, A. J., Colf, L. A., Hanick, N. A., Garcia, K. C., and Kranz, D. M. (2006) Engineering and characterization of a stabilized $\alpha1/\alpha2$ module of the class I major histocompatibility complex product Ld. *J. Biol. Chem.* **281,** 25734–25744 CrossRef Medline
17. Imarai, M., Goyarts, E. C., van Bleek, G. M., and Nathenson, S. G. (1995) Diversity of T cell receptors specific for the VSV antigenic peptide (N52–59) bound by the H-2Kb class I molecule. *Cell Immunol.* **160,** 33–42 CrossRef Medline
18. Mallis, R. J., Reinherz, E. L., Wagner, G., and Arthanari, H. (2016) Backbone resonance assignment of N15, N30 and D10 T cell receptor $\beta$ subunits. *Biomol. NMR Assign.* **10,** 35–39 CrossRef Medline
19. Liu, J., Tse, A. G., Chang, H. C., Liu, J. h., Wang, J., Hussey, R. E., Chishti, Y., Rheinhold, B., Spoerl, R., Nathenson, S. G., Sacchettini, J. C., and Reinherz, E. L. (1996) Crystallization of a deglycosylated T cell receptor (TCR) complexed with an anti-TCR Fab fragment. *J. Biol. Chem.* **271,** 33639–33646 CrossRef Medline
20. Pang, S. S., Berry, R., Chen, Z., Kjer-Nielsen, L., Perugini, M. A., King, G. F., Wang, C., Chew, S. H., La Gruta, N. L., Williams, N. K., Beddoe, T., Tiganis, T., Cowieson, N. P., Godfrey, D. I., Purcell, A. W., *et al.* (2010) The

structural basis for autonomous dimerization of the pre-T-cell antigen receptor. *Nature* **467,** 844–848 CrossRef Medline

21. Chou, P. Y., and Fasman, G. D. (1974) Prediction of protein conformation. *Biochemistry* **13,** 222–245 CrossRef Medline

22. Lee, D., Hilty, C., Wider, G., and Wüthrich, K. (2006) Effective rotational correlation times of proteins from NMR relaxation interference. *J. Magn. Reson.* **178,** 72–76 CrossRef Medline

23. García de la Torre, J., Huertas, M. L., and Carrasco, B. (2000) HY-DRONMR: prediction of NMR relaxation of globular proteins from atomic-level structures and hydrodynamic calculations. *J. Magn. Reson.* **147,** 138–146 CrossRef Medline

24. Hyberts, S. G., Arthanari, H., Robson, S. A., and Wagner, G. (2014) Perspectives in magnetic resonance: NMR in the post-FFT era. *J. Magn. Reson.* **241,** 60–73 CrossRef Medline

25. MacRaild, C. A., and Norton, R. S. (2014) RASP: rapid and robust backbone chemical shift assignments from protein structure. *J. Biomol. NMR* **58,** 155–163 CrossRef Medline

26. Rudolph, M. G., Speir, J. A., Brunmark, A., Mattsson, N., Jackson, M. R., Peterson, P. A., Teyton, L., and Wilson, I. A. (2001) The crystal structures of K^bm1 and K^bm8 reveal that subtle changes in the peptide environment impact thermostability and alloreactivity. *Immunity* **14,** 231–242 CrossRef Medline

27. Wieczorek, M., Abualrous, E. T., Sticht, J., Álvaro-Benito, M., Stolzenberg, S., Noé, F., and Freund, C. (2017) Major histocompatibility complex (MHC) class I and MHC class II proteins: conformational plasticity in antigen presentation. *Front. Immunol.* **8,** 292 CrossRef Medline

28. Palmer, A. G., 3rd, Kroenke, C. D., and Loria, J. P. (2001) Nuclear magnetic resonance methods for quantifying microsecond-to-millisecond motions in biological macromolecules. *Methods Enzymol.* **339,** 204–238 CrossRef Medline

29. Natarajan, K., McShan, A. C., Jiang, J., Kumirov, V. K., Wang, R., Zhao, H., Schuck, P., Tilahun, M. E., Boyd, L. F., Ying, J., Bax, A., Margulies, D. H., and Sgourakis, N. G. (2017) An allosteric site in the T-cell receptor Cβ domain plays a critical signalling role. *Nat. Commun.* **8,** 15260 CrossRef Medline

30. Teng, M. K., Smolyar, A., Tse, A. G., Liu, J. H., Liu, J., Hussey, R. E., Nathenson, S. G., Chang, H. C., Reinherz, E. L., and Wang, J. H. (1998) Identification of a common docking topology with substantial variation among different TCR-peptide-MHC complexes. *Curr. Biol.* **8,** 409–412 CrossRef Medline

31. van Zundert, G. C. P., Rodrigues, J. P. G. L. M., Trellet, M., Schmitz, C., Kastritis, P. L., Karaca, E., Melquiond, A. S. J., van Dijk, M., de Vries, S. J., and Bonvin, A. M. (2016) The HADDOCK2.2 web server: user-friendly integrative modeling of biomolecular complexes. *J. Mol. Biol.* **428,** 720–725 CrossRef Medline

32. Wang, J., Lim, K., Smolyar, A., Teng, M., Liu, J., Tse, A. G., Liu, J., Hussey, R. E., Chishti, Y., Thomson, C. T., Sweet, R. M., Nathenson, S. G., Chang, H. C., Sacchettini, J. C., and Reinherz, E. L. (1998) Atomic structure of an αβ T cell receptor (TCR) heterodimer in complex with an anti-TCR Fab fragment derived from a mitogenic antibody. *EMBO J.* **17,** 10–26 CrossRef Medline

33. Powell, L. D., Smith, K., and Hart, G. W. (1987) Site specific glycosylation patterns of H-2K: effects of allelic polymorphism and mitogenic stimulation. *J. Immunol.* **139,** 1206–1213 Medline

34. Shah, D. K., and Zúñiga-Pflücker, J. C. (2014) An overview of the intrathymic intricacies of T cell development. *J. Immunol.* **192,** 4017–4023 CrossRef Medline

35. Crump, A. L., Grusby, M. J., Glimcher, L. H., and Cantor, H. (1993) Thymocyte development in major histocompatibility complex-deficient mice: evidence for stochastic commitment to the CD4 and CD8 lineages. *Proc. Natl. Acad. Sci. U.S.A.* **90,** 10739–10743 CrossRef Medline

36. Tikhonova, A. N., Van Laethem, F., Hanada, K., Lu, J., Pobezinsky, L. A., Hong, C., Guinter, T. I., Jeurling, S. K., Bernhardt, G., Park, J.-H., Yang, J. C., Sun, P. D., and Singer, A. (2012) αβ T cell receptors that do not undergo major histocompatibility complex-specific thymic selection possess antibody-like recognition specificities. *Immunity* **36,** 79–91 CrossRef Medline

37. Johnson, J. L., Jones, M. B., Ryan, S. O., and Cobb, B. A. (2013) The regulatory power of glycans and their binding partners in immunity. *Trends Immunol.* **34,** 290–298 CrossRef Medline

38. Moody, A. M., Xiong, Y., Chang, H. C., and Reinherz, E. L. (2001) The CD8αβ co-receptor on double-positive thymocytes binds with differing affinities to the products of distinct class I MHC loci. *Eur. J. Immunol.* **31,** 2791–2799 CrossRef Medline

39. Delaglio, F., Grzesiek, S., Vuister, G. W., Zhu, G., Pfeifer, J., and Bax, A. (1995) NMRPipe: a multidimensional spectral processing system based on UNIX pipes. *J. Biomol. NMR* **6,** 277–293 Medline

40. Keller, R. (2004) *The Computer Aided Resonance Assignment Tutorial*, Cantina Verlag, Goldau, Switzerland

41. Salzmann, M., Pervushin, K., Wider, G., Senn, H., and Wüthrich, K. (1998) TROSY in triple-resonance experiments: new perspectives for sequential NMR assignment of large proteins. *Proc. Natl. Acad. Sci. U.S.A.* **95,** 13585–13590 CrossRef Medline

42. Shen, Y., and Bax, A. (2010) SPARTA+: a modest improvement in empirical NMR chemical shift prediction by means of an artificial neural network. *J. Biomol. NMR* **48,** 13–22 CrossRef Medline

43. R Core Team (2014) *R: a Language and Environment for Statistical Computing*, R Foundation for Statistical Computing, Vienna, Austria